Journal of Applied Physics

Step pinning and hillock formation in (Al,Ga)N films on native AlN substrates

Cite as: J. Appl. Phys. **132**, 223102 (2022); https://doi.org/10.1063/5.0125480
Submitted: 12 September 2022 • Accepted: 17 November 2022 • Published Online: 09 December 2022

T. Schulz, S.-H. Yoo, L. Lymperakis, et al.

Journal of Applied Physics ARTICLE scitation.org/journal/jap

Step pinning and hillock formation in (Al,Ga)N films on native AlN substrates

Cite as: J. Appl. Phys. **132**, 223102 (2022); doi: 10.1063/5.0125480
Submitted: 12 September 2022 · Accepted: 17 November 2022 ·
Published Online: 9 December 2022

T. Schulz,[1,a)] S.-H. Yoo,[2] L. Lymperakis,[2] C. Richter,[1] E. Zatterin,[3] A. Lachowski,[1] C. Hartmann,[1] H. M. Foronda,[4] C. Brandl,[4] H. J. Lugauer,[4] M. P. Hoffmann,[4] and M. Albrecht[1]

AFFILIATIONS

[1]Leibniz Institut für Kristallzüchtung, Max-Born Str. 2, 12489 Berlin, Germany
[2]Max-Planck-Institut für Eisenforschung GmbH, Max-Planck-Straße 1, 40237 Düsseldorf, Germany
[3]The European Synchrotron Radiation Facility (ESRF), Grenoble, France
[4]ams-OSRAM International GmbH, Leibnizstr. 4, 93055 Regensburg, Germany

[a)]**Author to whom correspondence should be addressed:** tobias.schulz@ikz-berlin.de

ABSTRACT

The influence of edge-type threading dislocations (TDs) on the epitaxial growth of AlGaN on native AlN substrates was investigated theoretically and experimentally. In the step flow growth regime, we find that pure edge-type TDs cause a pinning of surface steps, resulting in curved step segments. Theoretical calculations reveal that this pinning mechanism is solely mediated by the altered surface potential due the strain field imposed by the TD. Within the curved step segment, the step width is subject to changes resulting in an altered Ga/Al incorporation rate. According to the density functional theory calculation, this effect is related to the different surface diffusion length of Ga and Al and represents a further destabilization mechanism during step flow growth. Another consequence of surface step pinning is the occurrence of areas where the step width is increased. These areas serve as precursors for 2D nucleation due to an increased adatom density. Once nucleated, these nuclei grow along the c-direction via continuous 2D nucleation, while lateral expansion occurs due to adatom incorporation on the m-facets.

INTRODUCTION

In epitaxial growth, the precise control of surface morphology is of crucial importance for realizing abrupt interfaces and homogenous layers in semiconductor heterostructures. This necessitates an understanding of the growth mode, which dates back to the early models of Burton, Cabrera, and Frank.[1] Epitaxial growth may proceed via an initial 2D nucleation stage or due to incorporation of ad-atoms at pre-existing surface steps. These may be introduced by an appropriate surface preparation in the form of an intentional miscut angle or by means of threading dislocations (TDs) having a Burgers vector component parallel to the surface normal. Such TD-mediated surface step segments serving as additional incorporation sites may cause spiral growth, as it was first described in the works of Frank.[2] Threading dislocations without a Burgers vector component parallel to the surface normal may also influence the growth via their strain field causing pinning of surface steps. Such a blocking of surface steps or a local reduction in their propagation velocity causes irregular terrace widths in step-flow growth, as has been demonstrated for Si,[3] GaN,[4,5] and SiC.[6] In epitaxy of unitary or binary systems, this may result in surface roughening as a consequence of the varying adatom density on the terrace segments. In ternary compounds, such as AlGaN or InGaN, the situation is more complex since an irregular terrace width may additionally locally alter the composition owing to the different adatom diffusion lengths and, thus, incorporation probabilities at the step edges. These local composition changes due to pinning, thus, represent an additional stressor that further impacts on the step-flow growth. The consequences of strain-mediated pinning due to edge-type TDs in ternary compounds are far less explored, most likely owing to the typical high TD density in InGaN or AlGaN as a result of growth on, e.g., sapphire template substrates. The availability of native AlN substrates having TD densities on the order of $10^3\,\mathrm{cm}^{-2}$, as shown in Ref. 7, promises to study these issues in more detail. Step-flow growth of pseudomorphic AlN and high Al content $Al_xGa_{1-x}N$ films with a homogenous alloy composition

was demonstrated on such substrates.[8,9] The lower threading dislocation (TD) density, which reduces non-radiative recombination paths, enabled electrically injected laser diodes operating in the UV-C range.[10–12] However, despite appropriate growth conditions and miscut angles that yield step flow growth, the surface typically exhibits macroscopic hexagonal hillocks as shown in Refs. 13–15. The density of these hillocks varies but is typically in the range on the order of 10^3–10^4 cm^{-2}, which negatively impacts device characteristics.[14,15] In contrast to growth spirals observed on, e.g., high-temperature annealed AlN templates,[16] these hexagonal hillocks reveal a different surface step morphology and their formation mechanism is currently under debate. In this article, we combine atomic force microscopy (AFM), defect selective etching, cathodoluminescence (CL), transmission electron microscopy (TEM), and nano-beam scanning x-ray diffraction microscopy (SXDM) with density functional theory (DFT) to study the step-flow growth of high Al content AlGaN alloys on native AlN substrates. We demonstrate that pure edge-type TDs destabilize epitaxial step flow growth through pinning of surface steps. Due to the different diffusion lengths of Al and Ga, this additionally results in local deviations of the nominal composition as a result of the irregular terrace widths. Theoretical modeling of the adatom energetics at the step edge and the adatom kinetics show that all these effects are caused by the strain field imposed by TDs. Regions affected by pinning may serve as precursors for spontaneous 2D nucleation, which may ultimately lead to the growth of macroscopic, hexagonal hillocks.

EXPERIMENTAL AND COMPUTATIONAL DETAILS

$Al_{0.7}Ga_{0.3}N$ films are grown on 1-in. native AlN substrates (Hexatech) using metal organic vapor phase epitaxy (MOVPE). Nominally, such substrates exhibit a TD density of $<10^2$ cm^{-2}. Film thicknesses of 1 μm and 20 nm were realized using fluxes of 35 μmol/min TMAl and 15 μmol/min TMGa at a growth temperature of 1050 °C. The miscut angle of the AlN substrate was 0.2°. Nano-beam scanning x-ray diffraction (SXDM) experiments with an energy of 10188 eV were performed at the beamline ID01 of the European Synchrotron Radiation Facility (ESRF). The beam was focused using a tungsten Fresnel zone plate to a spot size of 45 nm, which was characterized in preliminary ptychography measurements on a Siemens star test structure. While the sample is scanned through the beam using a piezo stage, the area detector (MaxiPix), placed at a distance of 0.5 m, was read out continuously at 100 frames per second. Atomic force microscopy was performed using a Bruker Icon in the peak force mode with a tapping frequency of 0.3 Hz. Scanning electron microscopy (SEM) and cathodoluminescence (CL) studies were carried out in a Thermo Fisher Apreo using a Gatan Monarc system combined with a photomultiplier tube (Hamamatsu H11461). Spectrally resolved CL was carried out using a 1200 l/mm grating in combination with a Peltier cooled CCD camera (PIXIS). Defect selective wet etching experiments were conducted at 440 °C for 60 s using molten Ba (OH)2 as described in Ref. 17. Plan-view transmission electron microscopy (TEM) investigations were conducted in a FEI Titan 80–300 operated at 300 keV. Samples were prepared by mechanical polishing and final Ar^+ ion milling from 4 keV (incident angle 4°) down to 0.1 keV while increasing the milling angle to 10°.

RESULTS AND DISCUSSION

The surface topography of the 1 μm thick $Al_{0.7}Ga_{0.3}N$ was studied by AFM, as displayed in Figs. 1(a)–1(c). For the given growth conditions and miscut angles, the surface is characterized by monolayer height (c/2) surface steps with a terrace width of about 70 nm. The terrace width is slightly irregular, indicating minor deviations of the step edge orientation from the low energetic $\langle 11\bar{2}0\rangle$ directions. On a larger length scale, the surface additionally exhibits hexagonal hillocks with a height of around 40 nm and lateral diameter of about 10 μm, as can be seen in Fig. 1(b). The density of these hexagonal hillocks varies locally but is on the order of 10^4 cm^{-2}–10^5 cm^{-2} on average. The shapes of the hillocks are mirror-symmetric along the [1–100] miscut direction while being asymmetric along the [11–20] direction. A close up of one of the hillocks is displayed in Fig. 1(c) revealing concentric and closed growth terraces circumventing a depression near the tip of the hillock. Toward the bottom of the hillock, the terraces become more elliptical and elongated along the miscut direction. Concentric and closed terraces indicate that the hillocks are not related to spiral growth but rather grow along the [0001] direction via continuous 2D layer nucleation. Our observations and conclusions resemble those discussed in Ref. 13.

A series of monochromatic CL images between 235 and 285 nm (bandwidth 10 nm) of a hexagonal hillock is displayed in Fig. 2. While the emission from the layer has a maximum around 250 nm, the peak emission from the hillock is shifted toward longer wavelengths, evidencing the Ga enrichment. Moreover, dark lines on the side facets, which are aligned along the <11–20> directions (seen best at an emission around 265 nm), may indicate the presence of a misfit dislocation network or be a result of the perturbated step-flow growth conditions.

In addition to the prominent hexagonal hillocks described above, the panchromatic CL of the $Al_{0.7}Ga_{0.3}N$ film exhibits numerous smaller, parabolically shaped structures, as displayed in Fig. 3(a). The parabolas are aligned with their openings along the [1–100] miscut direction and appear in bright contrast. As we will discuss later in more detail, the intensity contrast is related to compositional changes, which affect the charge carrier confinement and, thus, the radiative recombination. The outer arms of the parabola merge into a horizontally aligned striped pattern, which is visible in the entire image.

Starting from the hypothesis that these features originate from TDs, we carried out defect selective etching experiments in the same region. A SEM image of the corresponding region is displayed in Fig. 3(b), showing a number of hexagonally shaped etch pits (see inset) evidencing TDs. The overall TD density varies from region to region but is in the order of 10^6 cm^{-2} on average. This is three to four orders of magnitude above the typical TD density of the bulk AlN substrate and, thus, leads to the conclusion that the majority of these TDs must have formed during the $Al_{0.7}Ga_{0.3}N$ epitaxy. Based on the calibration of our etching conditions and the size of the etch pits, we conclude that exclusively a-type dislocations with Burgers vectors $\mathbf{b} = 1/3 < 11–20>$ are present within the field of view. This is confirmed by detailed TEM experiments using the $\mathbf{g}\cdot\mathbf{b}$ criterion, as discussed in Sec. I in the supplementary material. Notably, the TDs occur in spatially close pairs or bundles

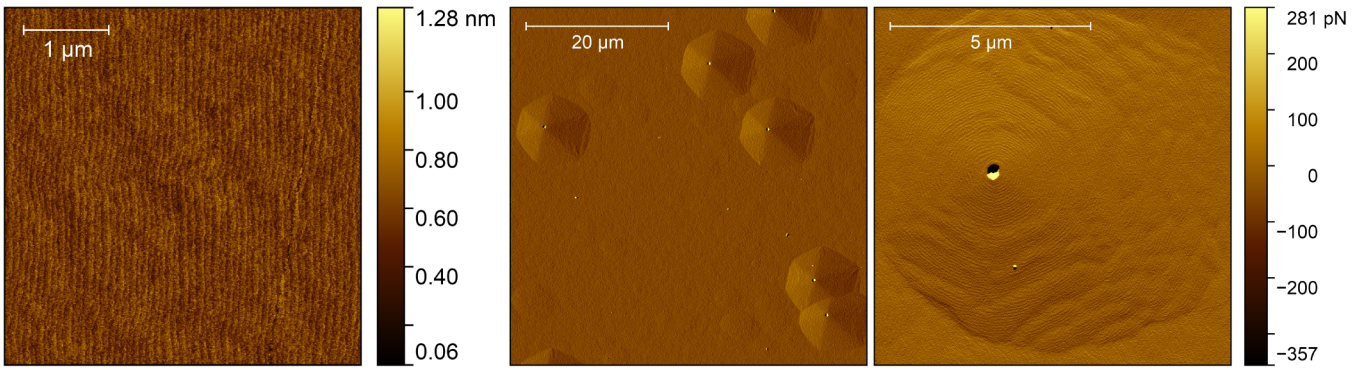

FIG. 1. (a) AFM image of the defect free surface. (b) and (c) Amplitude error recorded in different regions of a 1 μm $Al_{0.7}Ga_{0.3}N$ film.

consisting of an even larger number of TDs. Virtual connection lines between the pairs coincide with one of the three <1–100> directions. Similar pair-like edge-type TDs were observed in other epitaxial group III-N systems[18–21] referred to "hairpin" dislocations, forming at the interface.[22] Despite a TD density on the order of $10^6\,cm^{-2}$, the reciprocal space map (RSM) does not reveal any plastic relaxation of the film, as discussed in Sec. II in the supplementary material. Superimposing the positions of the etch pits with the panchromatic CL image in Fig. 3(a) (blue dots) reveals that each TD bundle is located at the vertex of a parabola. Notably, the intensity contrast in CL and the size of the parabola scale with the number of TDs within a bundle.

To trace the influence of TDs on step-flow growth back to its origin, we have investigated a 20 nm thick $Al_{0.7}Ga_{0.3}N$ layer, grown using otherwise identical conditions. A panchromatic CL image of the defect selectively etched film is displayed in Fig. 4(a), showing numerous similar, but much smaller parabolically shaped structures as for the 1 μm thick film. A zoomed in SEM and panchromatic CL image recorded simultaneously in a defect selectively etched region is displayed in Figs. 4(b) and 4(c). Analogous to the thick

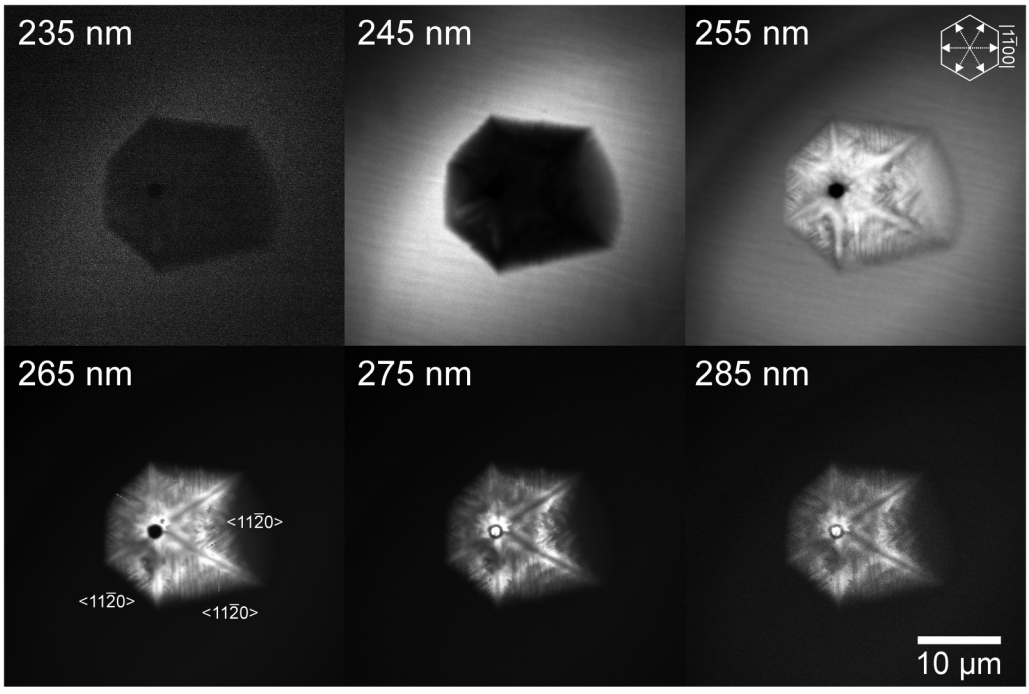

FIG. 2. Monochromatic CL with a bandpass of 10 nm of a large hexagonal hillock (5 keV, 1.6 nA).

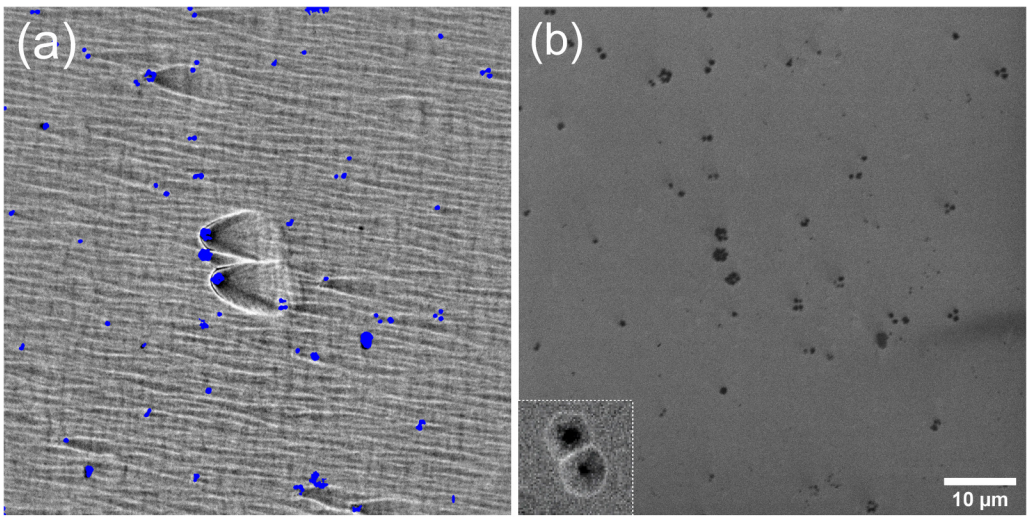

FIG. 3. (a) CL and (b) SEM image of a defect selectively etched $Al_{0.7}Ga_{0.3}N$ surface acquired simultaneously using 5 keV and a beam current of 0.8 nA. In (a), the CL image was superimposed with the position of the etch pits.

layer, each parabola is connected with TDs located at their vertex. In contrast to μm thick films, however, it is impossible to identify individual TDs of a bundle, since their spatial separation is smaller than the diameter of the etch pit. Still, counting the etch pits reveals a TD density of a comparable order of magnitude as for the 1 μm thick film. Thus, although the film thickness is only 20 nm, the TDs causing perturbations of step-flow growth form already at this very early growth stage.

We have analyzed the compositional changes within the parabolically shaped structures in more detail. Figure 4(d) shows the peak position of the CL emission obtained from deconvolution of the near bandgap emission using a Gaussian fit. We find that the parabolically curved region around the TD bundle is red-shifted and hence Ga-enriched. In the vicinity of the TD bundle, the red shift yields 100 meV, which evidences a substantially increased Ga content. At some distance from the TD bundle along the [1–100] miscut direction, periodic Ga-enriched line segments are visible in a regular arrangement. These become gradually smaller at larger distances from the TD bundle, indicating a diminishing perturbation of step-flow growth. More structural details about the region close to the TD bundle can be retrieved by TEM studies. Figure 4(e) shows a plan-view TEM image, using the g (−2110) reflection in the vicinity of a TD bundle. Here, the TD bundle is seen in the center of the image with the isolated edge-type TDs

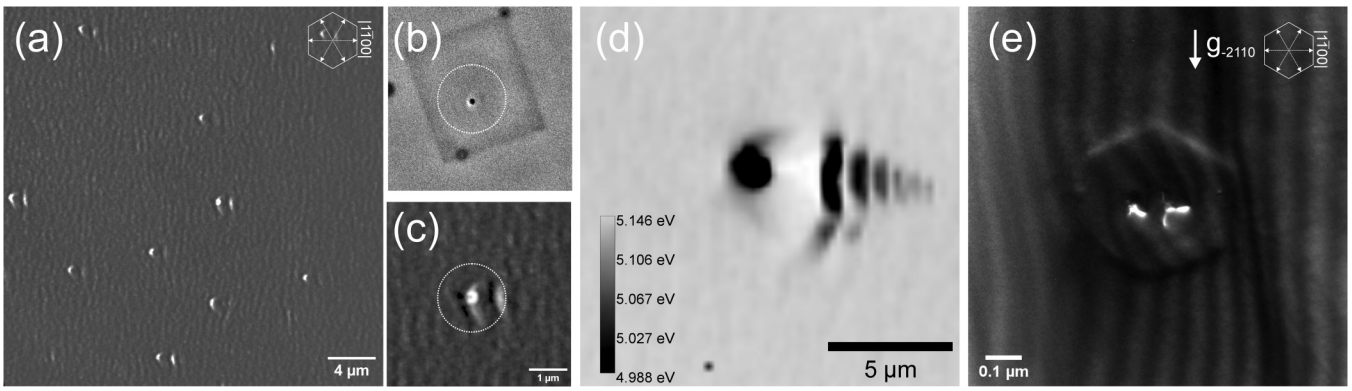

FIG. 4. (a) Panchromatic CL of a defect selectively etched 20 nm thick AlGaN film. (b) and (c) Zoomed in SEM and CL image recorded simultaneously in the region of an etch pit. (d) Spectrally resolved CL map of a 20 nm as-grown film, showing the peak emission energy as determined by a Gaussian fit. (e) Plan view TEM dark field of an initial 2D island image using the g (−2110) reflex. All SEM/CL images were recorded at 2 keV using a beam current of 1.6 nA.

appearing in bright contrast. Notably, the bundle is surrounded by a hexagonal structure, which can be identified as a nucleated island with fully developed m-facets. We have identified several other bundles, where comparable islands have nucleated. These observations suggest that the islands expand laterally via growth on the m-facets, while growth along the [0001] direction occurs via continuous 2D layer nucleation. Assuming a constant lateral growth rate, a hexagonal island with a diameter of about 500 nm as present in the 20 nm thick film would extend to a diameter of 22 μm for a film thickness of 1 μm. Such macroscopic sizes agree with the lateral dimensions of hillocks observed in our 1 μm thick film.

As discussed above, edge-type TDs have a significant impact on step flow growth. The way this manifests itself in CL studies in μm thick films can, however, be very different, ranging from smaller, parabolic structures up to macroscopic hillocks as a consequence of island nucleation. To confirm that all these perturbations can be traced back to edge-type TDs, we have carried out SXDM studies. To this end, we have measured the local strain of the AlN substrate by analyzing the AlN (02–25) reflection with the beam penetrating through the 1 μm thick $Al_{0.7}Ga_{0.3}N$ film. The characteristic Ga enrichment near the TDs in the film, e.g., as seen in Fig. 4(d), should, to first approximation, cause a small tensile-strained region in the underlying AlN substrate. Since the exact nature of this strain field is difficult to estimate, as it would require to include the strain caused by the TDs terminating at the interface, we will limit ourselves in the following investigations to the identification of a strain field with comparable properties. As the beam penetrates the epitaxial film, the presence of TDs in the substrate can additionally be probed.

In a first step, we have recorded a panchromatic CL image of the 1 μm thick $Al_{0.7}Ga_{0.3}N$ film, as displayed in Fig. 5(a). The image shows numerous growth perturbations of various sizes, ranging from smaller parabolas up to macroscopic, hexagonal hillocks. Figures 5(b) and 5(c) show the deflection of the AlN lattice planes obtained by analyzing the center of mass of the Bragg reflection in 2D cuts of reciprocal space maps. While "pitch" describes a change in the Bragg angle and is, therefore, a combined effect due to strain and rotation about an axis lying vertically in the image plane, "roll" can be interpreted as rotation about the horizontal axis. First, we note that our SXDM measurements confirm that the AlN substrate is free of TDs within the field of view, which corresponds to a TD density below 3×10^3 cm^{-2}. Due to the compositional changes in the region of growth perturbations (parabolas, hillocks), the substrates' lattice becomes strained, making the outer contours of all structures seen in CL also recognizable in the SXDM data. In addition, we notice small, tensile strained regions at the apexes of the parabolas as well as close to the geometric center of the larger hillocks. Magnified images in the region of a parabola apex and a hillock are displayed in Figs. 5(d)–5(i) for the CL, pitch and roll signal. Aside from the magnitude of the strain, we observe apparent similarities between the two regions in the SXDM data. An analysis of these strain fields clearly rules out the involvement of pre-existing TDs in the AlN substrate, as discussed in detail in Sec. II in the supplementary material. Instead, we relate these local

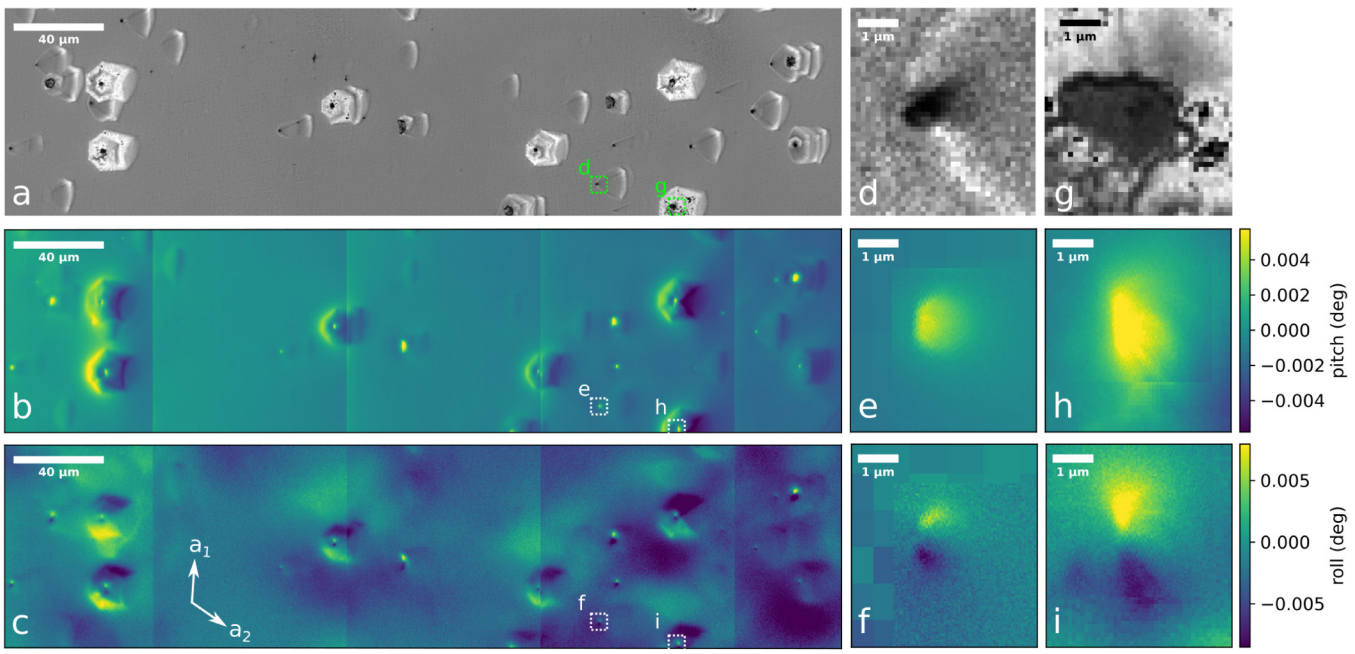

FIG. 5. Panchromatic CL at 5 keV using a beam current of 0.8 nA (a) and (b) and (c)nano x-ray diffraction measurements showing pitch and roll, respectively, referring to the rotation about the vertical and horizontal rotation that would be required to stay in Bragg condition. Dashed boxes in (a)–(c) mark the two zoomed in regions displayed in (d)–(f) and (g)–(i) for CL, pitch, and roll, respectively.

stressors to the characteristic Ga accumulation caused by edge-type TDs emerging from the AlN/AlGaN interface. Hence, this confirms a common mechanism for all growth perturbations, which is related to edge-type TDs.

Summarizing our experimental data, we find that TDs represent a severe perturbation of step flow growth, whereby affected regions are characterized by parabolically shaped, Ga-enriched regions or may serve as precursors for island nucleation. As these TDs are pure edge type, the impact on the step-flow growth must entirely be mediated by their strain field. In order to explain these observations, we will first focus on the smaller parabolical shaped structures, as observed in CL. Such parabolas, with their openings aligned along the step propagation direction, are indicative for pinning of surface steps, which results in curved step segments. In the following, we will demonstrate this effect by modeling the influence of the strain field of an edge-type TD on the surface energetics during step flow growth in the context of the Gibbs–Thomson effect.[3,23,24] For this purpose, we use a simple energy equilibrium consideration, which was successfully applied to study step propagation and pinning in the vicinity of edge-type TDs in various material systems.[3,23,24] Since we intend to give a qualitative description of pinning, in the following analysis, we do not distinguish between cation and anion species. The condition for the incorporation of surface adatoms at a step-edge kink, resulting in step propagation is given by

$$\Delta\mu > \Omega\, U_{(i,j)} + \beta \Delta L_{(i,j)}. \tag{1}$$

The left side of Eq. (1) contains the chemical potential $\Delta\mu$ of adatoms on the surface, which is proportional to supersaturation and, thus, constitutes the driving force for step propagation, i.e., growth. On the right side of the equation, Ω and $U_{(i,j)}$ refer to the atomic volume and the strain energy density, respectively, at a kink site with spatial coordinates (i,j). Finally, β is the step energy and $\Delta L_{(i,j)}$ is the increase in the step length upon incorporation and kink propagation. For a straight step, $\beta\Delta L_{(i,j)}$ equals zero, while it takes positive values for curved ones. To numerically solve Eq. (1), we form a rectangular mesh of nodes with indices (i,j) on a flat AlN terrace. Each node corresponds to the area of an III-N dimer. For each mesh element (i,j), we calculate the strain energy density $U_{(i,j)}$ arising from the superposition of two components: Biaxial compressive strain is equivalent to the lattice mismatch between the $Al_{0.7}Ga_{0.3}N$ film and the AlN substrate ($\epsilon_{xx} = \epsilon_{yy} = -0.8\%$), as in our experiment and strain energy due to an edge-type TD following elastic continuum theory in Ref. 25. For these calculations, we utilized linear interpolations for the lattice and elastic constants from Ref. 26. The resulting strain energy density is color coded in Fig. 6 with the TD located at the origin. To study the interplay between supersaturation $\Delta\mu$ and strain energy U on step propagation, we initially place a horizontal, straight step far from the dislocation line, i.e., at the bottom of Fig. 6. For $\Delta\mu = 0$, we consider that this straight step is in equilibrium with the environment and will neither propagate nor draw back. Then, the supersaturation is set to a positive value and Eq. (5) is evaluated for each node starting at the bottom right and moving to the left. If Eq. (1) for node (i,j) is fulfilled, the corresponding node (kink) is occupied. The procedure is repeated for all nodes in the corresponding row, until either the origin of the horizontal axis ($j = 0$) is reached or the respective mesh element does not satisfy inequality [Eq. (1)], i.e., the growth is blocked. Proceeding all mesh elements in such a way for different values of supersaturation $\Delta\mu$ results in the step edge profiles as shown in Fig. 6. For small values of supersaturation, the steps are pinned far from the dislocation line and exhibit a small curvature. As the supersaturation increases, the curvature increases, and the steps are pinned closer to the TD, which is expected due to the larger driving force for growth. For the highest supersaturation values of $\Delta\mu = 0.12$ eV, all mesh elements are occupied. Thus, in this case, the driving force for growth is large enough to overcome the energy barrier induced by the TD and pinning no longer occurs.

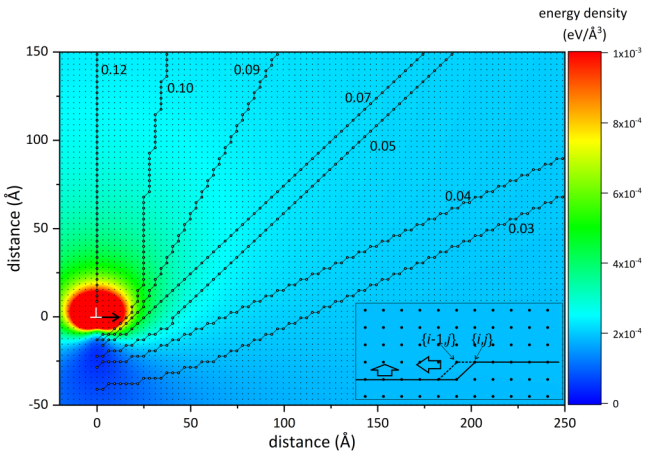

FIG. 6. Strain energy density around an edge type dislocation placed at the axes' origin of −0.8% biaxially strained AlN epilayer. The dotted curves indicate the step profiles for different values of supersaturation $\Delta\mu$ in units of eV/Å^3. The step edge energy is homogenous and equals 50 meV/Å. In Fig. 6, we plot the resulting step profiles using different values of $\Delta\mu$, which denotes the respective boundary between step propagation and step blocking. Inset: Schematic representation of a step edge with a kink at position (i,j) (solid line). The dashed lines indicate the updated kink position after its propagation leftward. The arrows indicate the directions of the kink (leftward) and step (upward) propagation.

Hence, the strain field of edge-type TDs may block the propagation of surface steps, resulting in curved step segments. This occurs as a consequence of the Gibbs–Thompson effect without the necessity of foreign impurities at the surface. It is reasonable to assume that the magnitude of step pinning scales with the number of TDs inside a bundle as a consequence of the increasing strain energy. While this model elucidates the effect of TDs on the shape of the surface steps, it cannot explain the compositional deviation in the curved segments as seen in CL or the nucleation of islands.

To gain insight into these issues, we have considered the surface kinetics of the Al and Ga adatoms in dependence of the terrace width. Terrace width alterations are expected to occur as a consequence of blocking, resulting in (i) step bunching or (ii) retained surface steps in the propagation direction. While the former effect reduces the terrace width, the latter enlarges it. In the first step, we have determined the Al and Ga diffusion barriers

TABLE I. Binding energies, diffusion barriers, and desorption limited residence time and diffusion lengths of Al and Ga adatoms on 2 × 2 N adatom (0001) AlN surfaces. For the calculation of the residence times and diffusion lengths, a temperature of 1350 K and an attempt frequency of 10^{14} Hz have been considered.

	Al	Ga
Binding energy (eV)	3.63	3.04
Kinetic barrier (eV)	2.14	1.82
Residence time (s)	0.3574	0.0021
Diffusion length (nm)	393	119

(E_{diff}) and binding energies (E_{bind}) on a flat (0001) AlN terrace with 2 × 2 N adatom surface reconstruction by employing DFT calculations[27,28] and the nudged elastic band (NEB) method.[29] This surface reconstruction is energetically most favorable under N-rich conditions.[30] From these energy values, we have calculated the desorption limited residence times and diffusion lengths for Al and Ga adatoms, respectively, for the experimental growth temperature of T = 1350 K, as summarized in Table I. More information on these calculations is provided in Sec. III in the supplementary material. The Al adatoms form more stable bonds and have higher kinetic barriers than Ga adatoms, which is related to stronger Al–N bonds. In total, this yields a more than two orders of magnitude larger desorption limited diffusion lengths for Al, as compared to Ga adatoms.

To estimate the influence of different diffusion lengths in the presence of step-pinning, we have modeled the adatom diffusion on a flat (0001) AlN terrace in dependence of the terrace width. The terrace is terminated by a step-up and a step-down edge while periodic boundary conditions are applied parallel to the step edge. (A detailed description of the simulation setup can be found in Sec. IV in the supplementary material.) At the step-up edge, the adatom incorporation probability is taken as unity, which corresponds to a perfect sink. At the step-down edge, we consider an arbitrary large Ehrlich–Schwoebel barrier, i.e., a mirror for adatoms. For simplicity, we further assume identical fluxes of Al and Ga impinging on the surface. Moreover, we consider quasi-steady-state conditions, i.e., the adatom diffusion is fast and the adatom density reaches equilibrium before step propagation. For the calculation, we build a hexagonal mesh of nodes on the terrace where each node coincides with a 2 × 2 surface cell. We solve the master equation,

$$\sum_j (-P(i \to j)c_i + P(j \to i)c_j) - \frac{c_i}{\tau_i} + \phi_i = 0, \qquad (2)$$

where $P(i \to j)$ is the jump probability per time from node i to a neighboring node j. c_i, τ_i, and ϕ_i denote the adatom density, residence time, and impinging flux at node i, respectively.

Solving Eq. (2) yields the Ga/Al ratio reaching the step-up edge as a function of the terrace width (and the equivalent miscut angle), as displayed in Fig. 7 (red curve). To a first approximation, this ratio will correlate with the composition of the growing AlGaN film. We find that the Ga/Al ratio increases with decreasing terrace width (or equivalently increasing miscut angle). The underlying reason for this effect stems from smaller Ga adatom desorption limited diffusion length as compared to Al. Thus, smaller terrace widths increase the amount of Ga adatom reaching the step-up edge, thus increasing the Ga content. This is in agreement with observations reported in Ref. 9, where a Ga content in the growing AlGaN film was found to increase for higher miscut angles. Since the pinning of surface steps results in step bunching in the curved step segments, these regions exhibit a reduced terrace width and, thus, a higher Ga content, which is in qualitative agreement with our CL data in Fig. 4(d).

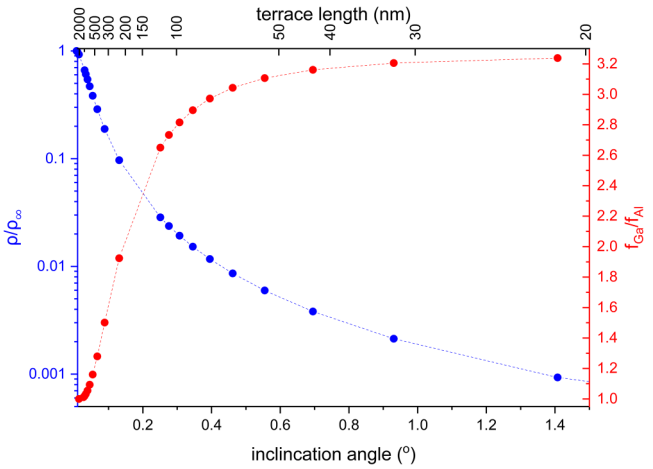

FIG. 7. Ga adatom density at the middle of the terrace (blue balls) and Ga over Al fluxes (red balls) toward the step as a function of the inclination angle. The density and fluxes on an arbitrary small inclination angle are used as a reference in both cases.

Nucleation of islands, leading to the growth of hexagonal hillocks, is generally promoted in areas having a larger terrace width. This can be expected to occur in the area that is confined between the arms of the curved step segments, as the TDs block the subsequent step flow into the area. To substantiate this, we have calculated the total adatom density in the middle of the terrace as a function of the terrace width (see blue dots in Fig. 7). Details of the calculation and analysis can be found in Sec. IV in the supplementary material. We find that the adatom density increases with increasing terrace width. For example, the adatom density increases by ×4 when the terrace length increases from 50 to 100 nm. Ultimately, this will promote spontaneous island nucleation in the area and, thus, explains the appearance of hexagonal hillocks in the vicinity of TDs.

CONCLUSIONS

In light of our results, we show that edge-type TDs cause a pinning of surface steps in AlGaN epitaxy. Based on theoretical considerations, we relate the pinning of initially straight surface steps that occurs to the strain energy induced by edge-type TDs as a result of the Gibbs–Thomson effect. The compositional changes and island nucleation, resulting in macroscopic hexagonal hillock in μm thick films, are a consequence of the altered terrace width due to pinning, which affects the adatom kinetics and densities of

Ga and Al. These compositional changes are prone to further perturbate step-flow growth in AlGaN films. Avoiding the TD bundles, whose origin is not fully clear at the moment, holds the premise of the undistorted step flow on native AlN substrates. Since these appear at an early growth stage and have very small misfit segments, they do not release much compressive strain in the AlGaN layer, except via their inclined threading arms. This suggests that their formation rather results from a contamination of the AlN surface or from subsurface damage. Alternatively, higher supersaturation will also reduce the effect of step pinning; however, the higher adatom fluxes will also increase the probability for spontaneous island nucleation and step bunching.

SUPPLEMENTARY MATERIAL

See the supplementary material for TEM analysis of threading dislocations, RSM data of the 1 μm thick AlGaN film, strain field simulations of various types of threading dislocations, as well as details about the theoretical modeling of the adatom diffusion and density on the terrace.

AUTHOR DECLARATIONS

Conflict of Interest

The authors have no conflicts to disclose.

Author Contributions

T. Schulz: Conceptualization (equal); Data curation (equal); Investigation (equal); Visualization (equal); Writing – original draft (equal); Writing – review & editing (equal). **S.-H. Yoo:** Data curation (equal); Investigation (equal); Writing – original draft (equal). **L. Lymperakis:** Data curation (equal); Investigation (equal); Writing – original draft (equal). **C. Richter:** Visualization (equal); Writing – original draft (equal). **E. Zatterin:** Investigation (equal); Writing – original draft (equal). **A. Lachowski:** Investigation (equal); Writing – original draft (equal). **C. Hartmann:** Investigation (equal). **H. M. Fornada:** Writing – original draft (equal). **C. Brandl:** Writing – original draft (equal). **H. J. Lugauer:** Supervision (equal); Validation (equal). **M. P. Hoffmann:** Writing – original draft (equal). **M. Albrecht:** Writing – original draft (equal).

DATA AVAILABILITY

The data that support the findings of this study are available from the corresponding author upon reasonable request.

REFERENCES

[1]W. K. Burton, N. Cabrera, F. C. Frank, and N. F. Mott, Philos. Trans. Proc. R. Soc. Lond. A. **243**, 299–358 (1951).
[2]F. C. Frank, Discuss. Faraday Soc. **5**(0), 48–54 (1949).
[3]A. Latyshev, H. Minoda, Y. Tanishiro, and K. Yagi, Jpn. J. Appl. Phys. **34**(Part 1, No. 10), 5768–5773 (1995).
[4]B. Heying, E. J. Tarsa, C. R. Elsass, P. Fini, S. P. DenBaars, and J. S. Speck, J. Appl. Phys. **85**(9), 6470–6476 (1999).
[5]F. Oehler, T. Zhu, S. Rhode, M. J. Kappers, C. J. Humphreys, and R. A. Oliver, J. Cryst. Growth **383**, 12–18 (2013).
[6]T. Kimoto, N. Miyamoto, and H. Matsunami, IEEE Trans. Electron Devices **46**(3), 471–477 (1999).
[7]R. Dalmau, J. Britt, H. Y. Fang, B. Raghothamachar, M. Dudley, and R. Schlesser, Mater. Sci. Forum **1004**, 63–68 (2020).
[8]I. Bryan, Z. Bryan, S. Mita, A. Rice, J. Tweedie, R. Collazo, and Z. Sitar, J. Cryst. Growth **438**, 81–89 (2016).
[9]I. Bryan, Z. Bryan, S. Mita, A. Rice, L. Hussey, C. Shelton, J. Tweedie, J.-P. Maria, R. Collazo, and Z. Sitar, J. Cryst. Growth **451**, 65–71 (2016).
[10]T. Sakai, M. Kushimoto, Z. Zhang, N. Sugiyama, L. J. Schowalter, Y. Honda, C. Sasaoka, and H. Amano, Appl. Phys. Lett. **116**(12), 122101 (2020).
[11]Z. Zhang, M. Kushimoto, T. Sakai, N. Sugiyama, L. J. Schowalter, C. Sasaoka, and H. Amano, Appl. Phys. Express **12**(12), 124003 (2019).
[12]Z. Zhang, M. Kushimoto, A. Yoshikawa, K. Aoto, L. J. Schowalter, C. Sasaoka, and H. Amano, Appl. Phys. Express **15**(4), 041007 (2022).
[13]I. Bryan, "Al-rich AlGaN and AlN growth on bulk AlN single crystal substrates," Ph.D. thesis (North Carolina State University, 2015).
[14]M. Kushimoto, Z. Zhang, Y. Honda, L. J. Schowalter, C. Sasaoka, and H. Amano, Jpn. J. Appl. Phys. **61**(1), 010601 (2022).
[15]Z. Zhang, M. Kushimoto, T. Sakai, N. Sugiyama, L. J. Schowalter, C. Sasaoka, and H. Amano, Appl. Phys. Express **12**(12), 124003 (2019).
[16]K. Uesugi, K. Shojiki, Y. Tezen, Y. Hayashi, and H. Miyake, Appl. Phys. Lett. **116**(6), 062101 (2020).
[17]L. Matiwe, C. Hartmann, L. Cancellara, M. Bickermann, A. Klump, J. Wollweber, S. Hagedorn, M. Weyers, and T. Straubinger, Phys. Status Solidi A **219**(7), 2100707 (2022).
[18]A. V. Lobanova, A. L. Kolesnikova, A. E. Romanov, S. Y. Karpov, M. E. Rudinsky, and E. V. Yakovlev, Appl. Phys. Lett. **103**(15), 152106 (2013).
[19]A. Tanaka, K. Nagamatsu, S. Usami, M. Kushimoto, M. Deki, S. Nitta, Y. Honda, M. Bockowski, and H. Amano, AIP Adv. **9**(9), 095002 (2019).
[20]M. Zhu, S. You, T. Detchprohm, T. Paskova, E. A. Preble, D. Hanser, and C. Wetzel, Phys. Rev. B **81**(12), 125325 (2010).
[21]A. Mogilatenko, A. Knauer, U. Zeimer, C. Netzel, J. Jeschke, R.-S. Unger, C. Hartmann, J. Wollweber, A. Dittmar, U. Juda, M. Weyers, and M. Bickermann, J. Cryst. Growth **505**, 69–73 (2019).
[22]D. M. Follstaedt, S. R. Lee, A. A. Allerman, and J. A. Floro, J. Appl. Phys. **105**(8), 083507 (2009).
[23]W. J. P. van Enckevort and A. C. J. F. van den Berg, J. Cryst. Growth **183**(3), 441–455 (1998).
[24]H. Omi, D. J. Bottomley, Y. Homma, T. Ogino, S. Stoyanov, and V. Tonchev, Phys. Rev. B **66**(8), 085303 (2002).
[25]J. P. Hirth, J. Lothe, and T. Mura, J. Appl. Mech. **50**(2), 476–477 (1983).
[26]M. A. Caro, S. Schulz, and E. P. O'Reilly, Phys. Rev. B **86**(1), 014117 (2012).
[27]G. Kresse and J. Hafner, Phys. Rev. B **47**(1), 558–561 (1993).
[28]G. Kresse and J. Furthmuller, Phys. Rev. B **54**(16), 11169–11186 (1996).
[29]G. Henkelman, B. P. Uberuaga, and H. Jónsson, J. Chem. Phys. **113**(22), 9901–9904 (2000).
[30]C. D. Lee, Y. Dong, R. M. Feenstra, J. E. Northrup, and J. Neugebauer, Phys. Rev. B **68**(20), 205317 (2003).